Received: 19 November 2024 | Revised: 8 January 2025 | Accepted: 12 January 2025

DOI: 10.1002/alz.14616

Alzheimer's & Dementia®
THE JOURNAL OF THE ALZHEIMER'S ASSOCIATION

RESEARCH ARTICLE

HDAC11 displays neuropathological alterations and offers as a novel drug target for Alzheimer's disease

Ping Bai[1,2] | **Prasenjit Mondal**[3] | **Yan Liu**[2] | **Ashley Gomm**[3] | **Claire Suen**[3] | **Liuyue Yang**[4] | **Biyue Zhu**[2] | **Haoqi Sun**[5] | **Chongzhao Ran**[3] | **Shiqian Shen**[4] | **Rudolph E. Tanzi**[3] | **Can Zhang**[3] | **Changning Wang**[2]

[1]Department of Respiratory and Critical Care Medicine, Targeted Tracer Research and Development Laboratory, West China Hospital, Sichuan University, Chengdu, China

[2]Athinoula A. Martinos Center for Biomedical Imaging, Department of Radiology, Massachusetts General Hospital, Harvard Medical School, Charlestown, Massachusetts, USA

[3]Genetics and Aging Research Unit, McCance Center for Brain Health, Mass General Institute for Neurodegenerative Disease, Department of Neurology, Massachusetts General Hospital, Harvard Medical School, Charlestown, Massachusetts, USA

[4]Department of Anesthesia, Critical Care and Pain Medicine, Massachusetts General Hospital, Harvard Medical School, Charlestown, Massachusetts, USA

[5]Department of Neurology, Beth Israel Deaconess Medical Center, Harvard Medical School, Boston, Massachusetts, USA

Correspondence
Ping Bai, Department of Respiratory and Critical Care Medicine, Targeted Tracer Research and Development Laboratory, West China Hospital, Sichuan University, Chengdu, Sichuan 610041, China.
Email: pingbai@scu.edu.cn

Can Zhang, Genetics and Aging Research Unit, McCance Center for Brain Health, Mass General Institute for Neurodegenerative Disease, Department of Neurology, Massachusetts General Hospital, Harvard Medical School, 114 16th Street, Charlestown, MA 02129, USA.
Email: zhang.can@mgh.harvard.edu

Changning Wang, Athinoula A. Martinos Center for Biomedical Imaging, Department of Radiology, Massachusetts General Hospital, Harvard Medical School, Charlestown, MA 02129, USA.
Email: CWANG15@mgh.harvard.edu

Funding information
NIH, Grant/Award Number: 1R01AG086433; Cure Alzheimer's Fund; Athinoula A. Martinos Center for Biomedical Imaging at the

Abstract

INTRODUCTION: Alzheimer's disease (AD) is characterized by amyloid pathology and neuroinflammation, leading to cognitive decline. Targeting histone deacetylase-11 (HDAC11) offers a novel therapeutic strategy due to its role in immune regulation.

METHODS: We conducted neuropathological analyses on human AD *post mortem* brain tissues and 5xFAD transgenic mice. We developed PB94, a brain-permeable HDAC11-selective inhibitor, and assessed its effects using live-animal imaging and behavioral studies.

RESULTS: HDAC11 was significantly upregulated in AD brains, correlating with amyloid pathology and neuroinflammatory markers. PB94 treatment reduced amyloid burden and neuroinflammation, improving cognitive function in 5xFAD mice.

DISCUSSION: Our findings highlight HDAC11 as a promising drug target for AD. PB94's ability to reduce amyloid pathology and neuroinflammation suggests its potential as an effective therapeutic. This study supports further exploration of HDAC11 inhibition as a treatment strategy for AD.

KEYWORDS
Alzheimer's disease, histone deacetylase-11, histone deacetylase-11 inhibitors, neuroinflammation

Ping Bai and Prasenjit Mondal contributed equally to this manuscript.

Massachusetts General Hospital; MADRC, Grant/Award Number: 1P30AG062421-01

Highlights

- Histone deacetylase-11 (HDAC11) is significantly upregulated in Alzheimer's disease (AD) brains and colocalizes with amyloid pathology and neuroinflammatory markers.
- Novel brain-permeable HDAC11-selective inhibitor PB94 demonstrates promising therapeutic potential for AD treatment.
- PB94 treatment reduces amyloid burden and neuroinflammation in AD mouse models, confirmed by live imaging studies.
- HDAC11 inhibition enhances microglial phagocytosis of amyloid beta proteins and modulates inflammatory cytokine levels.
- PB94 treatment improves cognitive function in AD mouse models while showing favorable brain penetration and selectivity.

1 | BACKGROUND

Alzheimer's disease (AD) is the most common neurodegenerative disease, affecting > 55 million people worldwide.[1,2] The progress of AD normally follows a continuum from asymptomatic stages with AD biomarker evidence, such as cerebral amyloid beta (Aβ) plaque accumulation and tau protein hyperphosphorylation, to mild cognitive and/or behavioral impairment, then AD-caused dementia.[3] Because AD is a complex neurological disorder that involves multiple pathological mechanisms, there is currently no cure. There are several biomarkers, including Aβ, tau, and neuroinflammatory regulators, that are regarded as potential therapeutic targets for AD treatment.[4–6] However, few agents targeting these biomarkers have been successfully approved for AD treatment in clinics. The failure of these agents in clinical trials can be attributed to the complex nature of the disease, the lack of understanding of its underlying mechanisms, the challenges of hitting specific targets in the brain, and limitations in clinical trial design.[1,7] Consequently, gaining a deeper understanding of the disease mechanisms as well as developing alternative approaches or targets are needed to discover a definitive solution for this devastating disorder.

Histone deacetylases (HDACs) are a family of epigenetic enzymes that regulate gene expression by removing acetyl groups from histone proteins, which determines the accessibility of DNA for transcription.[8,9] There are 11 subtypes of HDACs that have been identified in mammals, including class I (HDAC1, HDAC2, HDAC3, and HDAC8), class IIa (HDAC4, HDAC5, HDAC7, and HDAC9), class IIb (HDAC6, HDAC10), and class IV (HDAC11), and each of them is involved in various physiological processes.[10] Several studies have demonstrated that targeting HDAC activities holds promise as a therapeutic strategy for the treatment of AD.[11–14] For example, abnormal expression of HDAC6 was found in the AD brain, which can result in elevated hyperphosphorylation of tau and contribute to the formation of neurofibrillary tangles (NFTs) with subsequent neuronal dysfunction. HDAC6 inhibitors (HDAC6i) exhibited promising anti-AD potential by reducing neuroinflammation and ameliorating tau pathology.[15–17] These findings provide a new potential therapeutic strategy for AD associated with epigenetic mechanisms.

HDAC11 is a recently identified class IV HDAC member that has attracted great interest as a promising therapeutic target for many diseases.[18] Notably, it has been found that HDAC11 is highly expressed in the brain and plays a vital role in regulating immune response and inflammation.[19–22] The unique characteristics of HDAC11 have led us to raise a strong interest in its relationship to AD. However, due to the lack of knowledge of HDAC11 in AD and the absence of brain-penetrant HDAC11 inhibitors, little is known about the role of HDAC11 in the etiopathogenesis of AD and whether HDAC11 can be a potential therapeutic target for AD. To date, only a few HDAC11-selective inhibitors have been reported, yet none of them exhibited brain uptake nor showed therapeutic effects against AD.[19] Based on our previous work on developing HDAC inhibitors and positron emission tomography (PET) imaging probes,[23,24] we discovered a brain-permeable selective HDAC11 inhibitor named PB94. PB94 was evaluated to have significant inhibitory activity and selectivity toward HDAC11. Moreover, PB94 showed good brain uptake and drug-like profiles with favorable pharmacokinetic/pharmacodynamic properties, which could serve as an ideal agent for investigating the relationship between HDAC11 and AD. In this work, we carried out an array of studies both in vitro and in vivo to investigate the therapeutic potential of PB94 in AD. Meanwhile, we conducted an initial and exploratory investigation into the role and mechanistic aspects of HDAC11 in AD pathogenesis, which may advance the therapeutic development of targeting HDAC11 in AD.

2 | METHODS

All commercially available chemical reagents and solvents were ordered from commercial suppliers in American Chemical Society–grade purity or higher and directly used without further purification. [^{11}C]CO_2 (1.2 Ci) was obtained via the ^{14}N (p, α) ^{11}C reaction on nitrogen with 2.5% oxygen, with 11 MeV protons (Siemens Eclipse

RESEARCH IN CONTEXT

1. **Systematic review**: Alzheimer's disease (AD) affects > 55 million people worldwide, presenting a significant global health challenge. Despite decades of research, effective treatments remain elusive, primarily due to the complex etiology involving multiple pathological mechanisms, including amyloid beta (Aβ) plaques, tau protein hyperphosphorylation, and neuroinflammation. Traditional therapeutic approaches targeting these pathways have shown limited success in clinical trials, highlighting the need for novel therapeutic strategies. Recent research has identified epigenetic dysregulation as a crucial factor in AD pathogenesis, with histone deacetylases (HDACs) emerging as potential therapeutic targets. Among these, HDAC11, the most recently discovered member of the HDAC family, has gained attention due to its unique role in immune regulation and cellular processes, though its specific contribution to AD pathology remained largely unexplored until now.
2. **Interpretation**: This groundbreaking study provides compelling evidence for HDAC11 as a novel therapeutic target in AD. Analysis of human AD *post mortem* brain tissues and 5xFAD transgenic mice revealed significant upregulation of HDAC11, which notably correlated with amyloid plaques and neuroinflammatory markers. The development of PB94, a brain-permeable HDAC11-selective inhibitor, represents a significant advancement in targeting this mechanism. PB94 demonstrated remarkable efficacy in improving cognition and reducing amyloid pathology and neuroinflammation, as confirmed through live-animal chemiluminescence probing and positron emission tomography imaging. The study revealed that HDAC11 inhibition enhances the phagocytosis of Aβ proteins and decreases neuroinflammatory cytokines, suggesting a dual mechanism of action. These findings are particularly significant as they address both the accumulation of toxic proteins and the inflammatory response that characterizes AD progression.
3. **Future directions**: The identification of HDAC11 as a therapeutic target opens several promising research avenues. Future studies should focus on elucidating the precise mechanisms by which HDAC11 influences AD pathology, particularly its role in regulating neuroinflammation and amyloid clearance. The optimization of PB94 for clinical applications represents a critical next step, requiring detailed safety and efficacy studies in human subjects. Additionally, investigating the potential of HDAC11 inhibition in other neurodegenerative disorders could broaden the therapeutic applications of this approach. Long-term studies are needed to evaluate the sustained effects of HDAC11 inhibition and its impact on disease progression. Collaboration between academic institutions and pharmaceutical companies will be crucial for advancing these findings toward clinical applications, potentially leading to more effective treatments for AD patients.

cyclotron, Siemens Healthcare GmbH), and trapped on molecular sieves in a TRACER lab FX-MeI synthesizer (General Electric, GE Healthcare). $[^{11}C]CH_4$ was obtained by the reduction of $[^{11}C]CO_2$ in the presence of Ni/hydrogen at 350°C and recirculated through an oven containing I_2 to produce $[^{11}C]CH_3I$ via a radical reaction. Antibodies and dyes used in immunohistochemistry/immunocytochemistry (IHC/ICC) of this study are listed in Table 1.

2.1 | Cells and cell-based experiments

We used previously reported microglial BV2 cells[25] and tested whether PB94 may reduce microglia-related neuroinflammation using lipopolysaccharide (LPS), a well-characterized inflammatory inducer.[26] Briefly, BV2 cells were cultured following published methods and grew in Dulbecco's Modified Eagle Medium containing 10% heat-inactivated fetal bovine serum, 2 mM L-glutamine, and 1% penicillin/streptomycin (Life Technologies). BV2 cells were treated with dimethyl sulfoxide (DMSO; vehicle), Aβ (2 µg/mL)/10 ng/mL LPS alone or in combination with different concentrations (0–1000 nM) of PB94 in serum free medium for 24 hours. Subsequently, medium was collected and applied to lactate dehydrogenase (LDH) to assess cell viability; cells were extensively washed with phosphate-buffered saline (PBS) and were lysed in MPER (Mammalian Protein Extraction Reagent) lysis buffer supplemented with ethylenediaminetetraacetic acid–free protease inhibitors (Roche), Halt phosphatase inhibitor cocktail (ThermoFisher Scientific; $MPER^{++}$). Lysates were centrifuged at 12,000 × g at 4°C for 15 minutes and supernatants were collected and later applied to western blotting (WB) analysis.

For microglia related Aβ phagocytosis study, BV2 cells were cultured overnight and treated with DMSO (vehicle) or Aβ42 (2 µg/mL; from Anaspec/AS-24224) alone or in combination with different concentrations of PB94 in serum-free growth medium for 6 hours. Then, medium was collected to perform the LDH assay for cell cytotoxicity measurement. Cells were washed carefully with PBS twice, and lysed by adding 200 µL of $MPER^{++}$. Cell lysates were centrifuged at 12,000 × g at 4°C for 15 minutes and supernatants were collected for further studies. Total protein levels were quantified using the bicinchoninic assay (BCA) protein assay kit (Pierce).

2.2 | LDH assay

We performed the previously reported CytoTox-ONE assay to analyze cell viability by measuring the release of LDH[27] following manufacturer's guidelines (Promega). Briefly, 50 µL of cell culture media was used and a 1:1 dilution of substrate was added. The plate was incubated for 30 minutes in a 37°C incubator with the signal measured using a spectrophotometer at an excitation wavelength of 560 nm. Under the influence of the assay's substrate, resazurin was converted

TABLE 1 Overview of primary/secondary antibodies and dyes used in IHC/ICC of this study.

Primary antibodies and dyes	Host	Cat no. & supplier	Dilution
6E10	Mouse	803015, BioLegend	1:500
Anti-α-tubulin	Mouse	ab7291, Abcam	1:10000
IBA1	Rabbit	019-19741, Fujifilm Wako	1:500
IBA1	Goat	ab289874, Abcam	1:200
HDAC11	Mouse	Sc-390737, Santacruz	1:500
ASC	Rabbit	D2W8U, Cell signaling	1:1000
GFAP	Rat	13-0300, Invitrogen	1:500
3D6	Mouse	N/A, Eli Lilly	1:200
NeuN	Mouse	MAB377, Millipore Sigma	1:200
Hoechst	Dye	33342, Thermo Scientific	10 nM
Secondary antibodies			
Anti-Rat-A488	Donkey	Jackson Immuno Research	1:500
Anti-Mouse-A488	Donkey	A32766, Invitrogen	1:500
Anti-Rabbit-A594	Donkey	Jackson Immuno Research	1:500
Anti-Mouse-A640	Donkey	Jackson Immuno Research	1:500
Anti-Goat-A488	Donkey	ab150129, Abcam	1:500

Abbreviations: ASC, apoptosis-associated speck-like protein containing a caspase recruitment domain; GFAP, glial fibrillary acidic protein; IBA1, ionized calcium binding adaptor molecule 1; ICC, immunocytochemistry; IHC, immunohistochemistry; HDAC11, histone deacetylase-11.

to resorufin, its fluorescent form, due to LDH. The fluorometric results were used to compare the experiment group to the control group.

2.3 | Stereomicroscopic images before and after treatment on BV2 cells

Stereomicroscopic images were captured before and after the treatment of different compounds on BV2 cells to elucidate the cytotoxicity of compounds based on cellular morphology of BV2 cells.

2.4 | WB analysis

The previously described WB method was implemented to perform and analyze proteins of interest.[28] Briefly, cell lysates were collected, protein concentrations were measured by the BCA analysis and applied to the electrophoresis using the Novex NuPAGE SDSPAGE Gel System (Thermo Fisher Scientific), followed by membrane transfer, overnight primary antibody incubation at 4°C and 2 hour secondary antibody incubation at room temperature, followed by signal development. The house-keeping protein, β-actin, was used as an internal control. The Odyssey Fc with Image Studio was used for imaging.

2.5 | ICC staining of LPS induced BV2 cells

ICC assay was performed following previously published articles.[28] Briefly, BV2 cells were seeded and grown overnight in a LabTek 8-well glass chamber having 500 µL total volume of cells (≈ 100k). The cells were carefully washed with PBS twice at room temperature and then treated with DMSO, LPS (1 µg/mL), and with PB94 (1000 nM) for 3 hours in serum-free growth media. The media was discarded after 3 hours, then we washed each well carefully with PBS twice and fixed with 4% paraformaldehyde (PFA) for 20 minutes at room temperature. After that, we washed each well with 150 to 300 µL of PBS twice at room temperature and incubated with blocking buffer (5% Donkey serum with 0.1% Triton-X-100 in PBS). We then aspirated the blocking buffer and added 150 µL of primary antibody [mouse anti-α-tubulin antibody 0.5 µg/mL (DM1A;ab7291 abcam; 1:10000 dilution), Rabbit ionized calcium binding adaptor molecule 1 (IBA1; 019-19741 Fujifilm Wako; 1:500 dilution)] in each well and held at 4°C for overnight shaking. We then washed with washing buffer (PBS containing 0.1% Triton-X-100, 0.05% Tween-20) twice and incubated with specific secondary antibody (donkey anti-mouse a488 in 1:500 dilution, donkey anti-rabbit A594 in 1:500 dilution) in each well with gentle shaking for 2 hours at room temperature. Secondary solution was discarded and then we washed with washing buffer twice and incubated for 10 minutes with 20 nM of Hoechst solution for another 10 minutes at room temperature, washed with PBS twice, and finally mounted with Prolong Gold antifade reagent, dried at room temperature, and covered with a cover slip. For negative staining, instead of any primary antibody we used overnight incubation with blocking buffer and followed remaining procedures. Images were captured in different channels (405, blue [nucleus]; 488, green [α-tubulin]; 594, red [IBA1]) using a Nikon confocal microscope equipped with 40x oil objective.

2.6 | Meso Scale Discovery analysis (Aβ, inflammatory cytokines)[28]

Meso Scale Discovery (MSD) immunoassays, using the multiarray technology and electrochemiluminescence, are highly robust methods capable of identifying multiple proteins within a single sample. In this work, we performed MSD immunoassays using 4G8 and 6E10 MSD kits to assess Aβ phagocytosis in BV2 cells. These cells were exposed to Aβ (2 μg/mL) and PB94 compounds (0, 8 nM, 40 nM, 200 nM, and 1000 nM) to observe alterations in Aβ levels in the presence of our HDAC11 inhibitor. Additionally, we measured changes in inflammatory cytokine levels using multiplex MSD-cytokine assays, after induction of cells with LPS and subsequent treatment with PB94. For BV2 cells treated with vehicle, LPS, or PB94, both in the presence or absence of LPS, we used the MSD proinflammatory panel 1 (mouse) kits.

2.7 | Animal treatment

PB94 was dissolved in a solution of DMSO/Tween 80/saline (*v*/*v* = 1:1:8) to prepare a clear solution. Mice (6 months old) were divided into three groups (*n* = 4 per group): wild-type (WT) group, 5xFAD + PB94 group, and 5xFAD (vehicle) group. The 5xFAD + PB94 group received intraperitoneal injections of PB94 at a dose of 10 mg/kg body weight, once daily for 2 months. The WT and 5xFAD + vehicle groups received an equal volume of DMSO/Tween 80/saline vehicle daily for 2 months.

3 | BEHAVIORAL STUDY

3.1 | Y-maze

The Y-maze test is used for the assessment of memory and exploration behavior in rodents. It was conducted following previously described procedures.[29] Briefly, the mice were placed in a Y-maze apparatus that comprises three arms positioned at 120° angles. Prior to the testing, mice were allowed to explore only two of the three arms for 10 minutes, with the third arm (novel arm) blocked. Two hours later, the door to the novel arm was opened and the mice were tested for 5 minutes with access to all three arms. For statistics, the number of entries into the novel arm was counted.

3.2 | Buried food

The buried food test was conducted as previously described.[30] Briefly, mice were fed two pieces of sweetened cereal daily for two consecutive days ahead of the baseline test. On the testing day, after acclimation for 1 hour with a single cage, each mouse was placed in a clean home cage with a sweetened cereal pellet that was buried in the bedding with 5 cm in thickness. The latency of finding and consuming the food was counted to assess consciousness, awareness, and natural exploration behaviors.

3.3 | Novel object recognition

The novel object recognition (NOR) test was performed following previously described procedures.[31] Briefly, the mice were placed in a 50 × 50 cm acrylic glass box, and the exploration of the objects was recorded using SMART software 3.0 (Panlab). The mice were acclimated to the box for 5 minutes before the NOR test. The mice were then placed in the center of the box and allowed to explore two similar objects for 10 minutes, followed by returning to their home cage and resting for 10 minutes. When one of the previous two objects was replaced with a novel object, mice were placed into the box again and tested for another 10 minutes. The exploration time for each object was counted for statistics.

3.4 | In vivo chemiluminescence imaging

Male 5xFAD transgenic mice (6 months old) with or without PB94 treatment (10 mg/kg body weight intraperitoneal injections; once daily for 2 months), and male WT mice (6 months old) were shaved at the brain region. After conducting background imaging, the mice were intravenously injected with freshly prepared ADLumin-1 (4 mg/kg, 15% DMSO, 15% cremophor, and 70% PBS), and immediately observed under the IVIS Spectrum animal imaging system (PerkinElmer) with blocked excitation and open emission filter. The chemiluminescence signals were recorded at 0, 5, 10, 30, and 60 minutes postinjection (exposure time = 30 seconds, field of view = *D*). Living Image 4.2.1 software (PerkinElmer) was used to analyze the chemiluminescence signal of the brain regions of the mice.

3.5 | PET radiotracer synthesis

[^{11}C]PBR28 was prepared following a modified captive solvent method.[32] Briefly, in a solution of 1 mg radiolabeling precursor dissolved in 100 μL dimethylformamide in a 5 mL vial, [^{11}C]methyl iodide was bubbled through the reaction mixture for 3 minutes. After the reaction, purification was achieved via reverse-phase chromatography using a Gemini-NX C18 semi-preparative column with an isocratic mobile phase (MeCN:aqueous ammonium formate, *v*/*v* = 70:30). Subsequently, the product underwent solid-phase extraction (10% ethanol/saline) and sterile filtration. The identification of [^{11}C]PBR28 was carried out by co-injection with an unlabeled reference standard into the analytical high-performance liquid chromatography (Figure S1 in supporting information).

3.6 | PET/computed tomography imaging in rodents

The PET/computed tomography (CT) imaging studies in rodents were performed following our previous works.[33,34] Micro-PET/CT imaging

with [^{11}C]PBR28 was performed in 5xFAD (PB94) and 5xFAD (vehicle) mice. After intravenous injection of [^{11}C]PBR28 (3.7-5.6 Mbq per animal), a 60 minute dynamic PET acquisition was performed and followed by a 10 minute CT scan. PET data were reconstructed using a 3D-MLEM method, resulting in full width at a half-maximum resolution of 1 mm. These files were imported and analyzed using PMOD (PMOD 4.01, PMOD Technologies Ltd.).

3.7 | IHC study with paraffin embedded human brain sections

Eight μm thick paraffin embedded human brain sections (formalin fixed) were received from the Massachusetts Alzheimer's Disease Research Center (MADRC) and used for IHC analysis. These human control brain (Braak stage 0) and AD (Braak stage VI) sections from the hippocampal formation with lateral geniculate body and tail of the caudate nucleus region were deparaffinized following previously documented standard methods.[35] In brief, sections were washed three times with xylene (3 minutes each), followed by two times with 100% EtOH (2 minutes each), 95% EtOH (2 minutes), 70% EtOH (2 minutes), and finally 5 minutes of washing in running water. Antigen retrieval was achieved by placing these sections in a jar filled with sodium citrate buffer for 30 minutes in a water bath (95°C) followed by cooling the slides and wiping out excess liquid. Sections were encircled using a PAP pen and primary antibodies (HDAC11[rabbit], IBA1[goat], and 6E10 [mouse]) and secondary antibodies were added in different dilutions listed in table 1. Thereafter, slides were covered with cover slips after adding Prolong Gold antifade mounting reagent (P36934, Invitrogen). A Nikon C2 confocal microscope was used to capture images in different channels. Images were processed and analyzed using Image J.

3.8 | IHC study with mouse brain sections

The IHC study was conducted in accordance with established protocols following the Massachusetts General Hospital Institutional Animal Care and Use Committee protocol guidelines.[36] Male 5xFAD mice were used in this study and treated at the age of 6 months with vehicle (10% DMSO/10% Tween 80/80% saline) or PB94 (10 mg/kg, intraperitoneal injection; once daily for 2 months). Age- and sex-matched WT mice were also used and treated with vehicle. Vehicle and PB94 treated mice were euthanized and collected brains were incubated in 4% PFA for 28 hours at 4°C, followed by immersion in sucrose (30%) solution in PBS for cryoprotection. Using a sliding microtome, coronal brain sections were then dissected into 40 μm slices. Subsequently, these free-floating brain sections underwent a triple wash with PBS for 10 minutes each, followed by blocking with a solution containing 5% donkey serum and 0.1% Triton-X-100 in PBS for 1 hour. The sections were then incubated overnight with the appropriate primary antibodies as specified in table 1. After thorough washing with PBS, the sections were treated with suitable secondary antibodies for 2 hours at room temperature, followed by another triple wash with PBS. In cases in which thioflavin S (ThS) staining was necessary, the brain sections were incubated with a 0.1% ThS solution in PBS for an additional 10 minutes, followed by PBS washing until the solution was clarified. Subsequently, the sections were exposed to a 2 nM Hoechst solution for 10 minutes, followed by PBS washing. Finally, the brain sections were mounted onto glass slides using Prolong Gold antifade reagent, allowed to dry at room temperature, and covered with a cover slip. Different primary and secondary antibodies used in this work are listed in Table 1 with the exact dilution used.

3.9 | Data analysis

Confocal microscopic images were processed and analyzed using Image J software. Immunoblotting images were also analyzed using Image J software. All the results for different experiments in this work were shown as mean ± standard error of the mean. Statistical significance of the results was performed using Student two-tailed *t* test, one-way analysis of variance followed by a post hoc Tukey test in GraphPad PRISM. A P value of < 0.05 was considered statistically significant.

4 | RESULTS

4.1 | Pathological alterations of HDAC11 in AD brains

Previous studies indicated that HDAC11 plays a crucial role in neuroinflammation.[37] However, whether this epigenetic protein is associated with AD neuropathology is not yet clear. In this direction, we performed an IHC study with human *post mortem* healthy and AD brain sections (Braak stage 0 and VI, respectively) to observe the change in the expression level of certain biomarkers related to AD neuropathology. Figure 1A showed higher intensities of HDAC11, with microglia-specific IBA1 and Aβ1-16-responsive 6E10 that detects Aβ precursor protein (APP) in the *post mortem* AD brain section compared to healthy brain. Quantification of these images was shown in Figure 1B–D, which clearly indicated significantly higher expression of HDAC11 levels in AD brain sections and overlapping signals of HDAC11 with amyloid plaques and aggregates, suggesting a possible association of HDAC11 expression and amyloid deposition in AD neuropathology. Additionally, we performed immunostaining with WT and previously reported transgenic amyloid pathology model 5xFAD mice expressing APP$^{Swedish/Florida/London}$ and PS1$^{M146L/L286V}$ (Figure S2a,b in supporting information).[38] Our results revealed higher HDAC11 expression in 5xFAD mice (Figure S2c) recapitulating the results in human AD brains. Because HDAC11 is characterized with upregulation in AD human and transgenic brains, we reasoned that selective inhibition of HDAC11 with a potent inhibitor will ameliorate AD neuropathological changes. To test our hypothesis, we leveraged our recently developed brain-permeable HDAC11-selective inhibitor, PB94, and investigated its activity in different cellular and animal disease models to assess its efficacy on AD neuropathology.

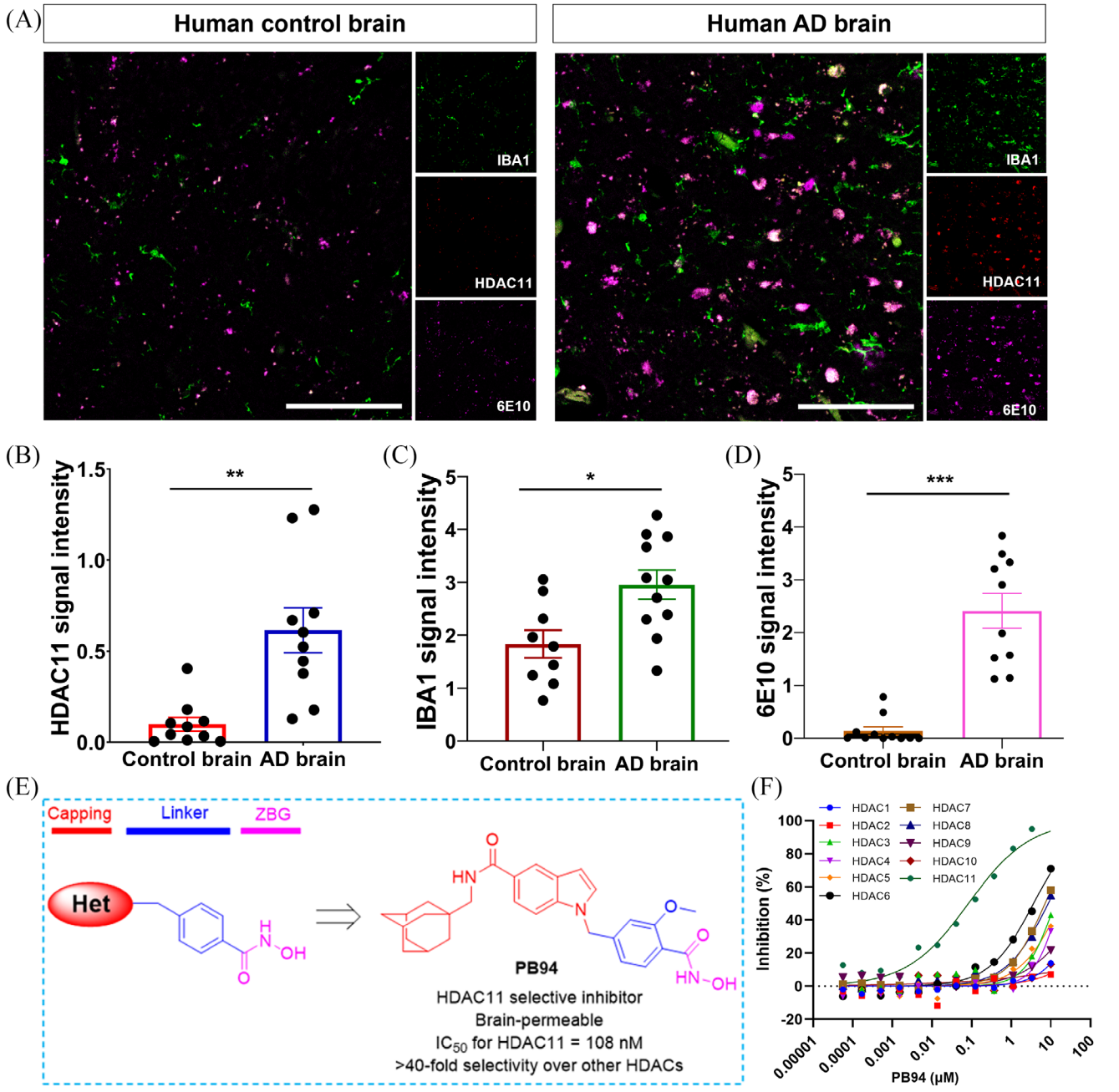

FIGURE 1 Pathological alterations of HDAC11 in association with AD hallmark amyloid pathology and neuroinflammation in the brain, which provides proof-of-concept developing small molecule inhibitors of HDAC11: (A) Human paraffin-embedded brain sections of AD and control cases were probed with microglia-specific IBA1, HDAC11-specific HDAC11, and APP/Aβ-specific 6E10 and images were captured in different laser channels (488, 594, and 640). Quantification of different biomarkers was calculated using Image J and shown in (B)–(D). (E), The design strategy of HDAC11-specific inhibitor, PB94, developed by introducing the rigid and lipophilic adamantane group into the capping group and a methoxy group on the phenol linker. (F), The inhibitory activity of PB94 against 11 different HDACs. Aβ, amyloid beta; AD, Alzheimer's disease; APP, amyloid beta precursor protein; HDAC11, histone deacetylase-11; IBA1, ionized calcium binding adaptor molecule 1

4.2 | Pharmacological and physicochemical properties of PB94

PB94 is an adamantane-based hydroxamic acid derivative that was discovered by the rational design of HDAC inhibitors.[36] The chemical structure of HDAC inhibitors generally contains three motifs: the capping group, zinc-binding group (ZBG), and the linker between them. Modification of each motif could alter the pharmacological and physicochemical properties of HDAC inhibitors. After structure–activity relationship (SAR) analysis and pharmacokinetic studies for our previously synthesized HDAC inhibitors, we found that introducing a rigid and lipophilic capping group significantly improved inhibitors' HDAC selectivity and brain permeability. Changing the substituents on the phenol linker could exert distinct inhibitory potency against HDAC iso-

forms. Following this rule, we developed a series of brain-permeable HDAC11 selective inhibitors and identified PB94 (Figure 1E) as the most promising one. PB94 exhibited good inhibitory activity and selectivity against HDAC11 with IC_{50} of 108 nM and over 40-fold selectivity over other HDAC isoforms (Figure 1F). Additionally, PB94 showed excellent brain permeability and metabolic stability in vivo in PET imaging studies in rodents, suggesting its great potential for central nervous system (CNS)–related disease treatment.[36] Moreover, our previous studies revealed that PB94 can reduce interleukin (IL)-10 expression in LPS-induced microglia BV2 cells and ease neuroinflammation in a neuropathic pain mouse model.[36] Given that PB94 has shown therapeutic potential for CNS-related disorders, we hypothesized that HDAC11 could be a good target for the development of potent therapeutics against AD.

4.3 | PB94 upregulates amyloid phagocytosis and downregulates inflammatory cytokines in cellular assays

In healthy brains, glial cells play a pivotal role in maintaining normal biological functions by clearing the amyloid aggregates through phagocytosis. In the early stages of AD development, Aβ proteins form aggregates and plaques, which accumulate in extracellular regions of the brain. This situation is exacerbated by glial cell dysfunction, which impairs the clearance of these plaques and cellular debris. The combination of Aβ accumulation and ineffective clearance mechanisms contributes to the progression of AD, ultimately leading to more severe manifestations of the disease. In this study, we used previously reported mouse microglia BV2 cells[28] to assess the effects of PB94 in upregulating the amyloid phagocytosis process. Overnight seeded BV2 cells (400k/mL on 6-well plates) were treated with different concentrations of PB94 in the presence/absence of Aβ42 (2 µg/mL). Confocal microscopic images were captured in bright fields before and after the treatment, and media were collected after 6 hours, followed by harvesting the cells with 200 µL of $MPER^{++}$ mixture. Confocal microscopic images showed no detrimental effects of PB94 in the presence/absence of Aβ (Figure S3a in supporting information), which suggested PB94-related safety. The strong tolerance of PB94 was further confirmed by the lack of significant differences of different doses of PB94 in our LDH analysis (Figure S3b). MSD-4G8 analysis showed significant upregulation of Aβ42 phagocytosis behavior at higher concentrations of PB94 (Figure 2A), though there were no significant changes in the Aβ42/Aβ40 ratios that further indicated possible degradation (Figure S3c).

4.4 | PB94 regulates cytokine levels in the presence of LPS-induced innate immunity activation in microglia BV2 cells

To assess the neuroinflammatory condition in the cellular system in the presence of PB94, LPS (10 ng/mL) was applied to BV2 cells with various concentrations of PB94 overnight. Stereomicroscopic images were captured before and after the treatment, and media were collected for further evaluation. Cells were harvested by adding 200 µL of $MPER^{++}$ solution followed by centrifugation at 12,000 × g for 20 minutes. Stereomicroscopic images before and after the treatment (Figure S3d) and LDH analysis (Figure S3e) showed no significant changes, respectively, in the cell morphology or the LDH release, which indicated no cytotoxicity of our compound PB94 on BV2 cells in the LPS-activated condition. Further, cell media were analyzed using MSD-cytokine analysis that showed significant reductions of cytokines IL-5, IL-10, and an increment of keratinocyte chemoattractant (KC)/growth-regulated oncogene (GRO) in the presence of PB94 (Figure 2B). Notably, IL-5 plays a crucial role in the activation of eosinophils that have significant contribution to allergic reactions and inflammatory responses associated with high eosinophil counts. IL-10 associates with various receptors and inhibits the synthesis of numerous cytokines that suppress Th1 proinflammatory responses and promote phagocytic uptake, whereas the chemokine KC/GRO (also known as CXCL1 in humans), primarily produced by fibroblasts and also expressed in macrophages and endothelial cells, is involved in neutrophil activation and shows hematopoietic activity during inflammation. Therefore, the significant reductions of cytokines IL-5, IL-10, and an increment of KC/GRO clearly indicated the effects of PB94 in protecting against neuroinflammation.

4.5 | In vitro analysis of microglia BV2 cells as a function of PB94

During AD progression, the microtubule network becomes severely damaged due to the hyperphosphorylation of tau protein. So, any molecule that can restore this damage or protect against this degeneration can be a potent drug candidate against AD. Hence, we have performed an ICC analysis using BV2 cells after treatment with PB94 to visualize the intracellular tubulin/microtubule network by assessing α-tubulin. Confocal images and quantification of these images revealed that PB94 led to a significant reduction of IBA-1 signal in the presence of LPS, supporting HDAC11 inhibition-related anti-neuroinflammation effects, but no such change was observed in α-tubulin expression, which indicates the healthy nature of tubulin/microtubules was maintained by PB94 treatment even in the presence of LPS (Figure 2C–E). In addition, we performed the WB assay with vehicle- and PB94-treated BV2 cell lysates, probed with HDAC11 and β-actin, which showed no significant changes in HDAC11 levels (Figure S4a,b in supporting information). This confirmed that PB94 is an HDAC11 inhibitor that doesn't significantly change HDAC11 expression levels.

Further, an ICC assay was performed using BV2 cells treated with the fluor 488-labeled Aβ42 (10 nM; from Anaspec/AS-60479) for 3 hours, in the presence/absence of PB94 (1000 nM) to visualize the impacts of PB94 on amyloid phagocytosis. Confocal microscopy images revealed higher intensities of amyloid signal from PB94 treated cells (Figure S5a in supporting information). Quantification of the images revealed that the number of amyloid-positive cells was significantly higher in association with PB94, which further confirmed the upregulation of amyloid phagocytosis in the presence of PB94 (Figure S5b).

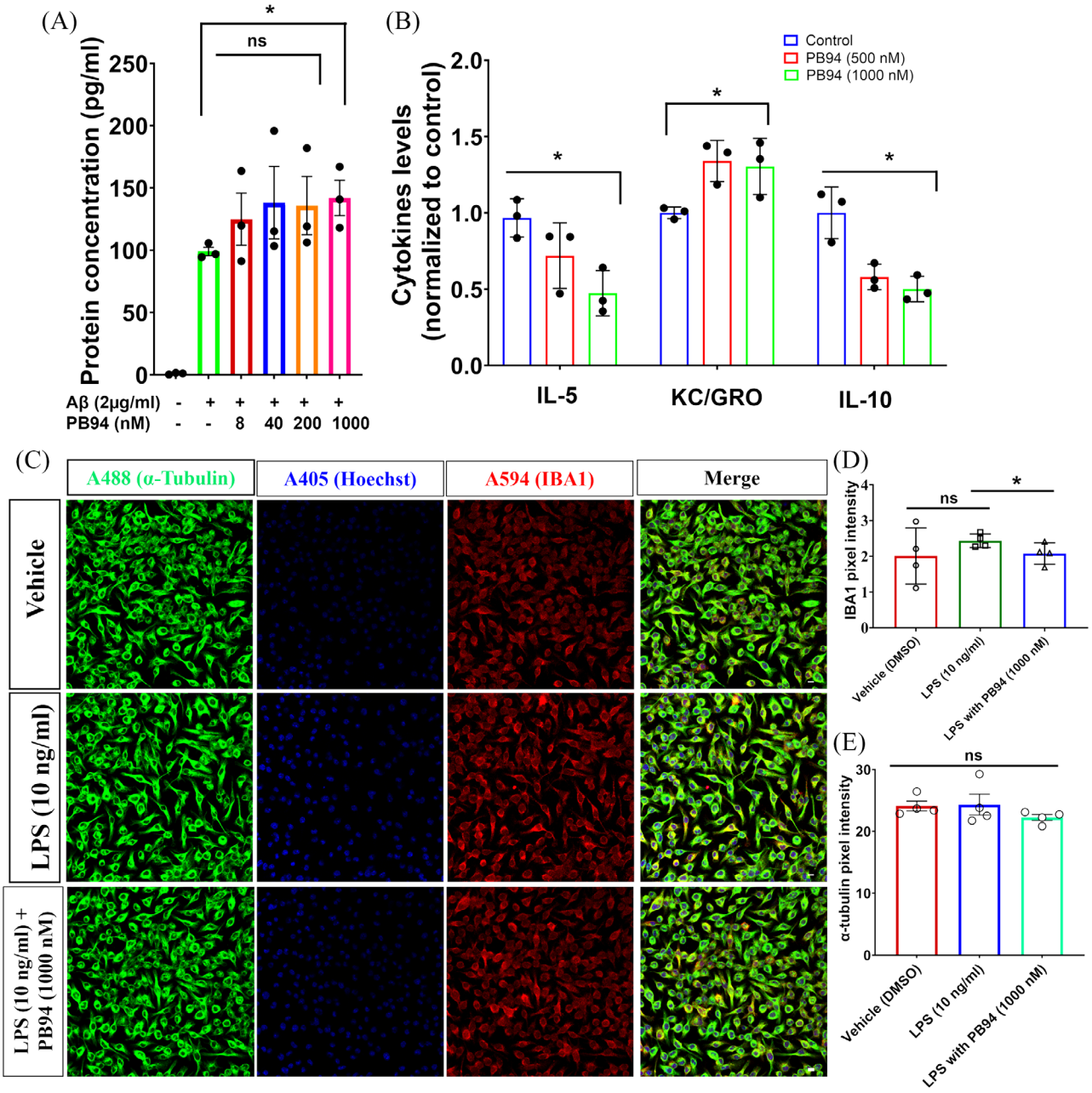

FIGURE 2 Effects of PB94 on mouse microglia BV2 cells in the presence of Aβ or LPS analyzed by MSD-cytokine analysis and immunocytochemistry: (A) Phagocytosis analysis revealed significant upregulation of phagocytosis in presence of PB94 (1000 nM); (B) MSD cytokine analysis revealed significant reduction of IL-5 and IL-10 with upregulation of KC/GRO cytokines; (C) confocal microscopy images were captured in different channels to assess the role of HDAC11 inhibitors on intracellular microtubule network. Images were captured in green (α-Tubulin), blue (Hoechst), and red (IBA1) channels to understand their expression levels. Quantification of α-Tubulin and IBA1 are shown in (D) and (E), respectively. Scale bars correspond to 10 μm. Data represented as $n = 3$. Aβ, amyloid beta; HDAC11, histone deacetylase-11; IBA1, ionized calcium binding adaptor molecule 1; IL, interleukin; KC/GRO, keratinocyte chemoattractant/growth-regulated oncogene; LPS, lipopolysaccharide; MSD, Meso Scale Discovery

4.6 | IHC analysis to assess the effects of PB94 on various amyloid and neuroinflammatory markers using AD transgenic and non-transgenic animals

Our studies indicated that HDAC11 plays a crucial role in neuroinflammation, which supported testing the potential effects of HDAC11 inhibitors on reducing AD-related symptoms to ultimately evolve as a novel and useful drug target for AD. As such, we further investigated the anti-AD impacts of PB94 using previously reported AD transgenic amyloid pathology model 5xFAD mice.[38] After treatment, mouse brains were used to perform IHC analysis by probing with glial fibrillary acidic protein (astrocyte) and 6E10 (amyloid pathology) and imaged under a Nikon confocal microscopy using a 4x objective (Figure 3A). The selective area within the image was further imaged in 40x to visu-

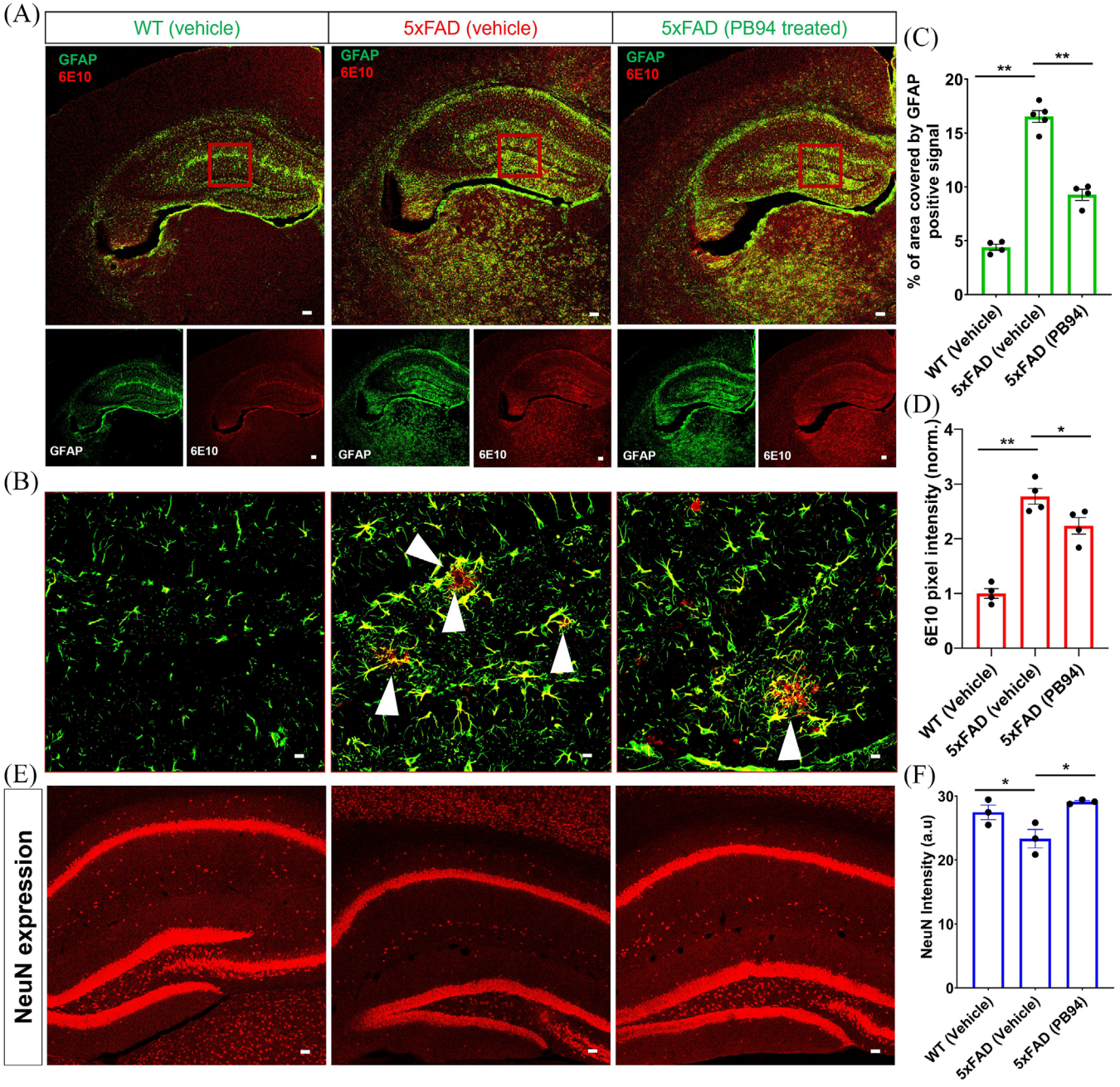

FIGURE 3 Assessment of PB94 on AD neuropathology using 5xFAD mice: (A) IHC confocal microscopy 4x images of WT (vehicle), 5xFAD (vehicle), 5xFAD (PB94) treated mouse brain sections stained with GFAP (astrocyte) and 6E10 (amyloid pathology). (B), Specific areas of images were magnified using 40x objective to reveal the interaction of amyloid deposition and astrocyte (interaction of amyloid aggregates and astrocytes are shown with white arrowheads). Quantification of the confocal images was measured using Image J and shown in (C) and (D). (E), Confocal microscopy (4x) images showed expression of NeuN-associated mature neurons of WT, 5xFAD (vehicle), and 5xFAD (PB94) treated mouse brain sections, with corresponding quantification of the images shown in (F). AD, Alzheimer's disease; GFAP, glial fibrillary acidic protein; IHC, immunohistochemistry; WT, wild type

alize the amyloid plaques surrounded by astrocytes (Figure 3B). The white arrowheads within the section in Figure 3B show the region of amyloid and astrocyte expression in the brain section that reduced in PB94-treated mouse brain sections. Quantification of the images suggested that treatment with PB94 significantly reduced the percentage of the area of astrocyte-positive signal and amyloid-positive signal intensity (Figure 3C,D). Further, the NeuN-positive signal showed a significant increase of mature neurons around the hippocampal area after PB94 treatment on AD transgenic mice (Figure 3E), which was further confirmed by quantifying the images (Figure 3F).

In addition, we performed more IHC analyses by incubating these brain sections using amyloid plaque–specific 3D6, microglia-specific IBA1, 6E10, and the inflammasome activation hallmark protein ASC (apoptosis-associated speck-like protein containing a caspase recruit-

ment domain [CARD]).[39] In neurodegenerative diseases, ASC is closely associated with neuroinflammation by playing a key role in nucleotide-binding domain, leucine-rich repeat, and pyrin domain–containing protein 3 inflammasome activation and upregulating the production of pro-inflammatory cytokines, where its activation within microglia can contribute to neuronal damage and disease progression through chronic inflammation. Confocal microscopic (4x) images are shown in Figure 4A, and further magnification of these images was captured using 10x objective, shown in Figure 4B (left panel 3D6; right panel IBA1). Quantification of these images showed a significant reduction of number of amyloid plaques, size and burden (% area), and microglia intensity in PB94-treated brain sections (Figure 4C–F). In addition, we performed another IHC analysis by probing the WT, 5xFAD (vehicle), and 5xFAD (PB94 treated) with ASC-specific ASC antibody, and Aβ/APP-specific 6E10 antibody to analyze the pathological change in AD mouse brains. Confocal microscopy images (4x) are shown in Figure 4G. Quantification of these images showed not only a reduction of average plaque size but also total plaque number and percentage area covered by the amyloid positive signals from PB94-treated brain sections compared to vehicle-treated 5xFAD mice (Figure 4H–J). Neuroinflammation-associated ASC burden (%) and the size of ASC aggresome were significantly reduced in PB94-treated 5xFAD mouse brain sections. Confocal images and related quantification are shown in Figure 4K–L. We also assessed the effects of PB94 on HDAC11 expression by IHC using 5xFAD mouse brain sections and analyzed with the Image J. Quantification of the images revealed that PB94 did not significantly change HDAC11 expression levels in different sub-regions, including hippocampal CA3 and dentate gyrus of 5xFAD mice (Figure S6 in supporting information). This suggested that PB94 led to anti-AD effects in 5xFAD mice by functioning as an HDAC11 inhibitor without significantly changing HDAC11 expression levels.

4.7 | PB94 attenuates amyloid burden and behavioral deficits in AD transgenic animals

Brain Aβ plaque accumulation is one of the most striking features in AD pathology. Our previous work has identified ADLumin-1 as a brain-permeable chemiluminescence probe that can precisely detect plaques in vivo.[40] Thus, to examine whether PB94 can ease the Aβ burden in vivo, chemiluminescence imaging studies with ADLumin-1 were performed. As shown in Figure 5A, compared to the WT animal group, a significantly increased chemiluminescence signal of ADLumin-1 in 5xFAD mouse brains was observed, suggesting the accumulation of the Aβ plaques in 5xFAD mice. Medication with PB94 showed reduced signal of ADLumin-1 in 5xFAD mouse brains, indicating that PB94 can ameliorate the amyloid burden (Figure 5B). Our findings of reduced amyloid pathology in AD mice raised intriguing possibilities that pharmacologic inhibition of HDAC11 might provide therapeutic benefits to restore cognitive functions. To investigate this, we administered PB94 in 5xFAD mice and conducted an array of cognitive behavior assessments. 5xFAD mice were treated with PB94 (10 mg/kg) daily and performed behavioral tests, including Y-maze, buried food, and NOR tests on day 14. As shown in Figure 5C, the 5xFAD mice displayed a prolonged latency in finding buried food to intake compared to WT mice, which was significantly shortened by the PB94 treatment. Additionally, compared to the control vehicle, PB94-treated 5xFAD mice showed improved performances in the Y-maze and NOR tests, suggesting the anti-AD potential of PB94 by improving integrated cognitive functions in 5xFAD mice.

4.8 | Anti-inflammatory effects of PB94 using [^{11}C]PBR28 probe

HDAC11 was reported to be involved in the immune response.[41–43] Thus, we performed PET imaging studies with the well-reported translocator protein (18 kDa; TSPO)-targeting probe, [^{11}C]PBR28,[44,45] to determine the anti-neuroinflammation effects of PB94 in AD (Figure 5D). Dynamic PET scans were conducted in 5xFAD (vehicle) and 5xFAD (PB94) mice (Figure 5E). The summed PET/CT images and time–activity curves (TACs) revealed high uptake of [^{11}C]PBR28 in the brains of 5xFAD (vehicle) mice, with a maximum standardized uptake value of 1.2 (Figure 5F). Regional analysis indicates the regions of the hippocampus, thalamus, hypothalamus, and striatum have a relatively high uptake of [^{11}C]PBR28, corresponding to the neuroinflammation in these regions. Of note, 5xFAD mice treated with PB94 exhibited significantly declined radioactivity (≈ 41%) accumulation in the whole brain and each region compared to 5xFAD (vehicle), demonstrating the anti-inflammation effects of PB94 (Figure 5G,H). Collectively, our multi-modal investigations showed strong anti-AD impacts of PB94 including improved neurobehavioral functions associated with reduced neuroinflammation and ameliorated amyloid pathology related to AD.

5 | DISCUSSION

Despite extensive research, effective treatments for AD remain elusive, largely due to the multifaceted nature of AD. Our current study provides compelling evidence for the potential of HDAC11 as a novel therapeutic target in AD. Our findings reveal a marked upregulation of HDAC11 in both human AD *post mortem* brain tissues and 5xFAD transgenic mouse brains, correlating with the presence of amyloid plaques and neuroinflammatory markers. This observation aligns with previous studies that have implicated epigenetic dysregulation in neurodegenerative diseases.[11,12] The co-localization of HDAC11 with Aβ pathology suggests that HDAC11 may play a crucial role in the neuroinflammatory processes that exacerbate AD. By selectively inhibiting HDAC11 with PB94, we observed significant reductions in amyloid burden and neuroinflammation, as evidenced by live-animal chemiluminescence probing and PET imaging.

The pharmacological properties of PB94, including its brain permeability and selectivity for HDAC11, are noteworthy. Previous HDAC inhibitors have faced challenges related to poor brain penetration and lack of isoform specificity. PB94's favorable pharmacokinetic profile positions it as an ideal candidate for investigating the therapeutic

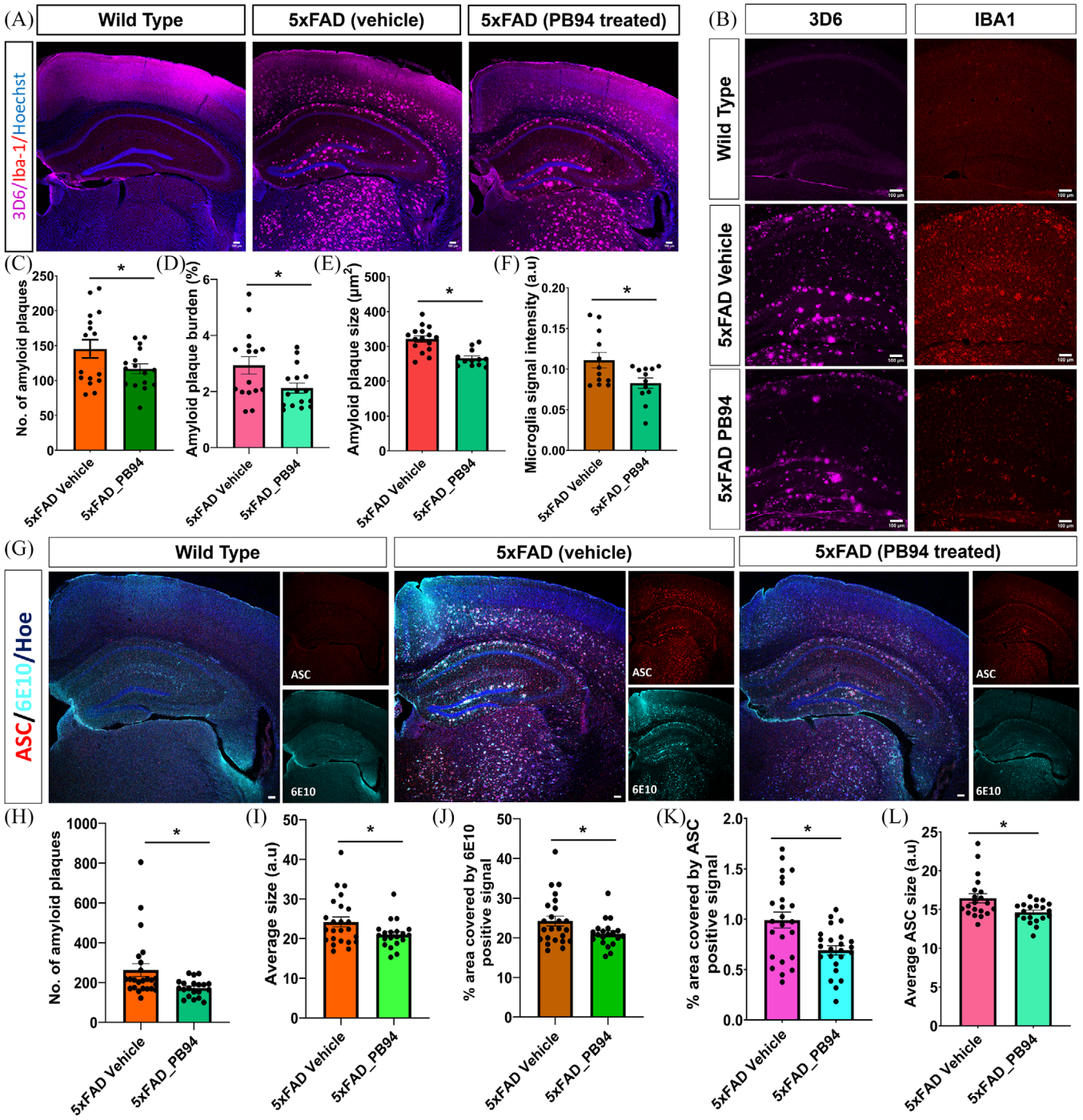

FIGURE 4 IHC confocal microscopy analysis to further assess amyloid and neuroinflammatory events as a function of PB94 in 5xFAD animal brain sections. (A), 4X confocal microscopy images of WT (vehicle), 5xFAD (vehicle), and PB94 treated 5xFAD mouse brain sections were probed with amyloid-specific 3D6, microglia-specific IBA1, and nuclei-specific Hoechst to observe the effects of PB94 on amyloid pathology. (B), Higher magnification (10x) images of the WT, 5xFAD sections are shown in magenta (3D6) and red (IBA1). Quantification of the images to measure the expression of different biomarkers is shown in (C)–(F). (G), 4X confocal microscopy images of WT (vehicle), 5xFAD (vehicle), and PB94 treated 5xFAD mouse brain sections were probed with ASC, 6E10, and Hoechst to observe the effects of PB94 on neuroinflammasome activity in association with amyloid neuropathology in the brain. Quantification of the images to measure the expression of different biomarkers is shown in (H)–(L). Scale bars corresponded to 100 μm. IBA1, ionized calcium binding adaptor molecule 1; IHC, immunohistochemistry; WT, wild type

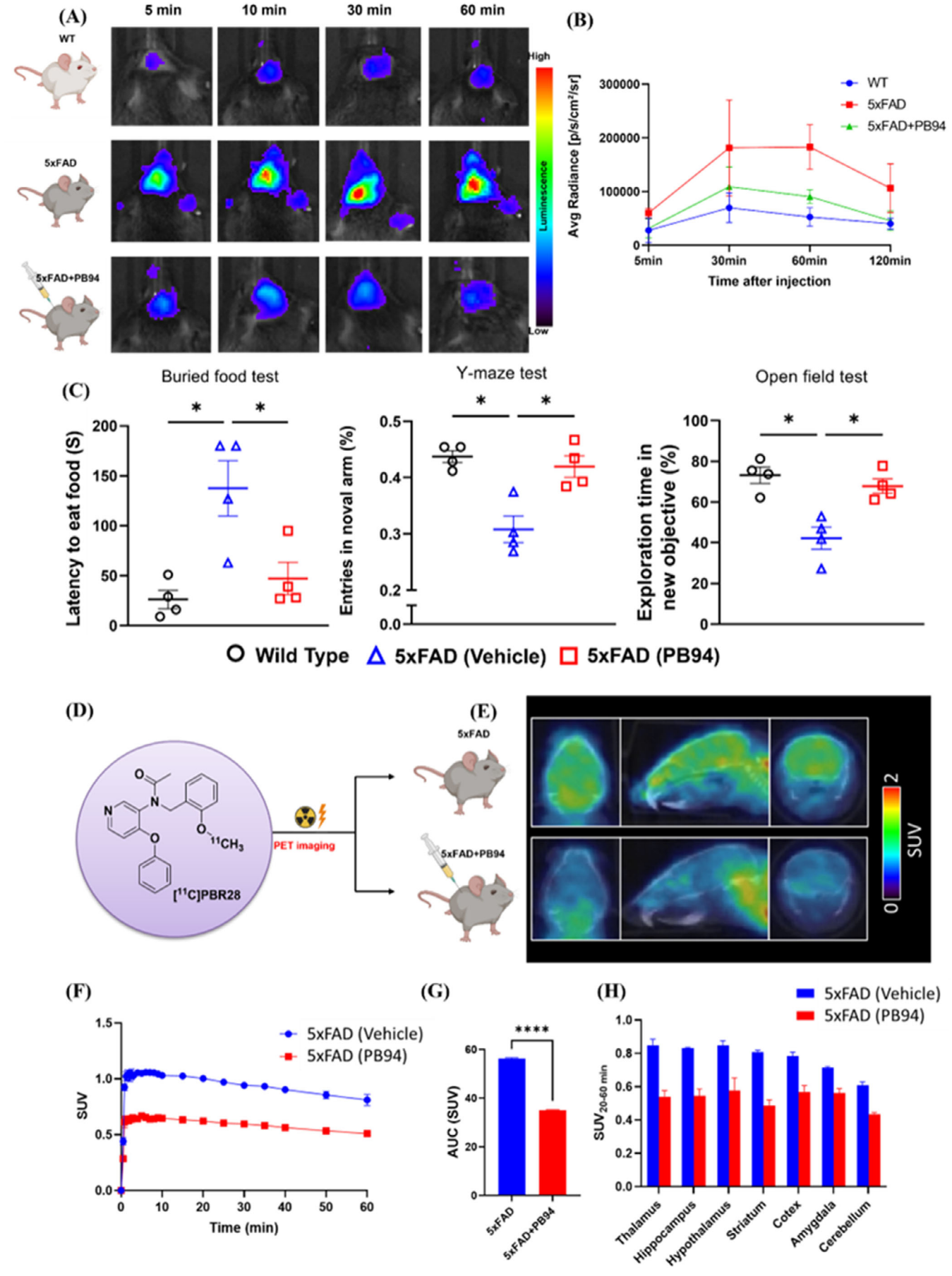
(A)
5 min
10 min
30 min
60 min
WT
5xFAD
5xFAD+PB94
High
Luminescence
Low
(B)
Avg Radiance [p/s/cm²/sr]
300000
200000
100000
0
WT
5xFAD
5xFAD+PB94
5min
30min
60min
120min
Time after injection
(C)
Buried food test
Latency to eat food (S)
200
150
100
50
0
Y-maze test
Entries in noval arm (%)
0.5
0.4
0.3
0.2
0.0
Open field test
Exploration time in new objective (%)
100
80
60
40
20
0
Wild Type
5xFAD (Vehicle)
5xFAD (PB94)
(D)
PET imaging
[11C]PBR28
(E)
5xFAD
5xFAD+PB94
SUV
2
0
(F)
SUV
1.5
1.0
0.5
0.0
5xFAD (Vehicle)
5xFAD (PB94)
0
10
20
30
40
50
60
Time (min)
(G)
****
AUC (SUV)
60
40
20
0
5xFAD
5xFAD+PB94
(H)
5xFAD (Vehicle)
5xFAD (PB94)
SUV20-60 min
1.0
0.8
0.6
0.4
0.2
0.0
Thalamus
Hippocampus
Hypothalamus
Striatum
Cotex
Amygdala
Cerebellum

FIGURE 5 Reduction of amyloid pathology and restoration of cognitive functions in 5xFAD animals as a function of PB94. (A), Chemiluminescence imaging studies with ADLumin-1 showed a reduction of amyloid burden in AD-transgenic animals after administering PB94 in the disease model. (B), Average radiation of ADLumin-1 shows a reduction of signal intensity in PB94-treated 5xFAD mice compared to vehicle-treated WT/5xFAD. (C), PB94 improves cognitive function in AD-transgenic animals as shown by battery behavior tests. $N = 4$ mice, one-way analysis of variance followed by post hoc Tukey test to determine the difference among groups. (D), The chemical structure of [^{11}C]PBR28. (E), Representative PET/CT images (30–60 minutes) focused on the 5xFAD- and PB94-treated 5xFAD mouse brain. (F), TACs of [^{11}C]PBR28 in WT and 5xFAD mice whole brain. (G), The AUC of TACs showed significantly increased radioactivity accumulation in the whole brain of AD mice. H, Reginal analysis showed the uptake of [^{11}C]PBR28 significantly increased in regions of interest. AD, Alzheimer's disease; AUC, area under the curve; CT, computed tomography; PET, positron emission tomography; SUV, standardized uptake value; TACs, time–activity curves; WT, wild type.

potential of HDAC11 inhibition in AD. Our biochemical and immunohistochemical analyses further elucidate the mechanisms by which PB94 exerts its effects, including enhanced phagocytosis of Aβ proteins and decreased levels of neuroinflammatory cytokines. The upregulation of Aβ phagocytosis in microglial BV2 cells treated with PB94 highlights the potential of HDAC11 inhibition to restore the normal function of glial cells in clearing amyloid aggregates. This is particularly relevant given that glial dysfunction contributes to the accumulation of Aβ plaques in the early stages of AD.

Notably, neuroinflammation plays a complex dual role in the pathogenesis of AD. In the early stages, the inflammatory response helps clear amyloid aggregates, but as the disease progresses, this response transforms into a destructive process. HDAC11 may play a critical role in regulating this transition. By appropriately inhibiting HDAC11 activity, we may be able to slow or intervene in the pathological progression of AD, thereby providing protection for patients' cognitive functions. While previous studies have focused on other HDAC isoforms, such as HDAC6, our study is among the first to demonstrate the efficacy of HDAC11 inhibition in an AD model. This novel approach not only addresses the amyloid hypothesis but also targets the neuroinflammatory processes that contribute to cognitive decline.

Collectively, this study establishes HDAC11 as a viable therapeutic target for AD and presents PB94 as a potent, brain-permeable HDAC11 inhibitor with significant anti-AD effects. By demonstrating the ability of HDAC11 inhibition to ameliorate multiple aspects of AD pathology, including amyloid burden, neuroinflammation, and cognitive deficits, our findings open new avenues for epigenetic-based interventions in AD. Continued exploration of HDAC11's roles in AD and the refinement of PB94 could significantly advance the field, ultimately improving outcomes for individuals affected by this devastating disorder.

ACKNOWLEDGMENTS

This work was supported in part by NIH grants 1R01AG086433 (CZ and CW), the Cure Alzheimer's Fund (CZ and CW), and a pilot funding from the Athinoula A. Martinos Center for Biomedical Imaging at the Massachusetts General Hospital (CW) and MADRC grant (1P30AG062421-01).

CONFLICT OF INTEREST STATEMENT

C.W., P.B., C.Z., S.S., and R.E.T. are co-inventors of the HDAC11 inhibitor used in this publication. Other co-authors have no conflicts of interest to declare. Author disclosures are available in the supporting information.

ETHICS STATEMENT

All animal studies were carried out at Massachusetts General Hospital (PHS Assurance of Compliance No. A3596-01, USA). The Subcommittee on Research Animal Care (SRAC) serves as the Institutional Animal Care and Use Committee (IACUC) for the Massachusetts General Hospital (MGH). SRAC reviewed and approved all procedures detailed in this paper.

REFERENCES

1. 2023 Alzheimer's disease facts and figures. *Alzheimers Dement*. 2023;19(4):1598-1695.
2. Goedert M, Spillantini MG. A century of Alzheimer's disease. *Science*. 2006;314(5800):777-781.
3. Porsteinsson AP, Isaacson RS, Knox S, Sabbagh MN, Rubino I. Diagnosis of early Alzheimer's disease: clinical practice in 2021. *J Prev Alzheimers Dis*. 2021;8(3):371-386.
4. Nortley R, Korte N, Izquierdo P, et al. Amyloid beta oligomers constrict human capillaries in Alzheimer's disease via signaling to pericytes. *Science*. 2019;365(6450):eaav9518.
5. Sato C, Barthelemy NR, Mawuenyega KG, et al. Tau kinetics in neurons and the human central nervous system. *Neuron*. 2018;98(4):861-864.
6. Heneka MT, Carson MJ, El Khoury J, et al. Neuroinflammation in Alzheimer's disease. *Lancet Neurol*. 2015;14(4):388-405.
7. Khan S, Barve KH, Kumar MS. Recent advancements in pathogenesis, diagnostics and treatment of Alzheimer's disease. *Curr Neuropharmacol*. 2020;18(11):1106-1125.
8. Bird A. Perceptions of epigenetics. *Nature*. 2007;447(7143):396-398.
9. Seto E, Yoshida M. Erasers of histone acetylation: the histone deacetylase enzymes. *Cold Spring Harb Perspect Biol*. 2014;6(4):a018713.
10. Sengupta N, Seto E. Regulation of histone deacetylase activities. *J Cell Biochem*. 2004;93(1):57-67.
11. Graff J, Rei D, Guan JS, et al. An epigenetic blockade of cognitive functions in the neurodegenerating brain. *Nature*. 2012;483(7388):222-226.
12. Graff J, Tsai LH. Histone acetylation: molecular mnemonics on the chromatin. *Nat Rev Neurosci*. 2013;14(2):97-111.
13. Peleg S, Sananbenesi F, Zovoilis A, et al. Altered histone acetylation is associated with age-dependent memory impairment in mice. *Science*. 2010;328(5979):753-756.
14. Jakovcevski M, Akbarian S. Epigenetic mechanisms in neurological disease. *Nat Med*. 2012;18(8):1194-1204.
15. Ding H, Dolan PJ, Johnson GV. Histone deacetylase 6 interacts with the microtubule-associated protein tau. *J Neurochem*. 2008;106(5):2119-2130.
16. Fukada M, Hanai A, Nakayama A, et al. Loss of deacetylation activity of Hdac6 affects emotional behavior in mice. *PLoS One*. 2012;7(2):e30924.

17. Govindarajan N, Rao P, Burkhardt S, et al. Reducing HDAC6 ameliorates cognitive deficits in a mouse model for Alzheimer's disease. *EMBO Mol Med*. 2013;5(1):52-63.
18. Gao L, Cueto MA, Asselbergs F, Atadja P. Cloning and functional characterization of HDAC11, a novel member of the human histone deacetylase family. *J Biol Chem*. 2002;277(28):25748-25755.
19. Liu SS, Wu F, Jin YM, Chang WQ, Xu TM. HDAC11: a rising star in epigenetics. *Biomed Pharmacother*. 2020;131:110607.
20. Buglio D, Khaskhely NM, Voo KS, Martinez-Valdez H, Liu YJ, Younes A. HDAC11 plays an essential role in regulating OX40 ligand expression in Hodgkin lymphoma. *Blood*. 2011;117(10):2910-2917.
21. Deubzer HE, Schier MC, Oehme I, et al. HDAC11 is a novel drug target in carcinomas. *Int J Cancer*. 2013;132(9):2200-2208.
22. Sun L, Marin de Evsikova C, Bian K, et al. Programming and regulation of metabolic homeostasis by HDAC11. *EBioMedicine*. 2018;33:157-168.
23. Wang C, Schroeder FA, Wey HY, et al. In vivo imaging of histone deacetylases (HDACs) in the central nervous system and major peripheral organs. *J Med Chem*. 2014;57(19):7999-8009.
24. Strebl MG, Campbell AJ, Zhao WN, et al. HDAC6 Brain Mapping with [(18)F]Bavarostat enabled by a Ru-mediated deoxyfluorination. *ACS central science*. 2017;3(9):1006-1014.
25. Zhang C, Griciuc A, Hudry E, et al. Cromolyn reduces levels of the Alzheimer's disease-associated amyloid beta-protein by promoting microglial phagocytosis. *Sci Rep*. 2018;8(1):1144.
26. Liang F, Wan Y, Schaak D, et al. Nanoplasmonic fiber tip probe detects significant reduction of intracellular Alzheimer's disease-related oligomers by curcumin. *Sci Rep*. 2017;7(1):5722.
27. Choi SH, Bylykbashi E, Chatila ZK, et al. Combined adult neurogenesis and BDNF mimic exercise effects on cognition in an Alzheimer's mouse model. *Science*. 2018;361(6406):eaan8821.
28. Mondal P, Bai P, Gomm A, et al. Structure-based discovery of a small molecule inhibitor of histone deacetylase 6 (HDAC6) that significantly reduces Alzheimer's disease neuropathology. *Adv Sci*. 2024;11(1):e2304545.
29. Zhou X, Wu X, Wu Y, et al. Indole-3-propionic Acid, a gut microbiota metabolite, protects against the development of postoperative delirium. *Ann Surg*. 2023;278(6):e1164-e1174.
30. Yang L, Ding W, Dong Y, et al. Electroacupuncture attenuates surgical pain-induced delirium-like behavior in mice via remodeling gut microbiota and dendritic spine. *Front Immunol*. 2022;13:955581.
31. Lueptow LM. Novel object recognition test for the investigation of learning and memory in mice. *J Vis Exp*. 2017;(126):55718.
32. Zurcher NR, Loggia ML, Mullett JE, et al. [(11)C]PBR28 MR-PET imaging reveals lower regional brain expression of translocator protein (TSPO) in young adult males with autism spectrum disorder. *Mol Psychiatry*. 2021;26(5):1659-1669.
33. Bai P, Lan Y, Wang H, et al. Synthesis and characterization of a positron emission tomography imaging probe selectively targeting the second bromodomain of bromodomain protein BRD4. *Bioconjugate Chem*. 2021;32(8):1711-1718.
34. Bai P, Lan Y, Patnaik D, et al. Design, synthesis, and evaluation of thienodiazepine derivatives as positron emission tomography imaging probes for bromodomain and extra-terminal domain family proteins. *J Med Chem*. 2021;64(19):14745-14756.
35. Jaisa-Aad M, Munoz-Castro C, Healey MA, Hyman BT, Serrano-Pozo A. Characterization of monoamine oxidase-B (MAO-B) as a biomarker of reactive astrogliosis in Alzheimer's disease and related dementias. *Acta Neuropathol*. 2024;147(1):66.
36. Bai P, Liu Y, Yang L, et al. Development and Pharmacochemical characterization discover a novel brain-permeable HDAC11-selective inhibitor with therapeutic potential by regulating neuroinflammation in mice. *J Med Chem*. 2023;66(23):16075-16090.
37. Dai Y, Wei T, Shen Z, Bei Y, Lin H, Dai H. Classical HDACs in the regulation of neuroinflammation. *Neurochem Int*. 2021;150:105182.
38. Oakley H, Cole SL, Logan S, et al. Intraneuronal beta-amyloid aggregates, neurodegeneration, and neuron loss in transgenic mice with five familial Alzheimer's disease mutations: potential factors in amyloid plaque formation. *J Neurosci*. 2006;26(40):10129-10140.
39. Prather ER, Gavrilin MA, Wewers MD. The central inflammasome adaptor protein ASC activates the inflammasome after transition from a soluble to an insoluble state. *J Biol Chem*. 2022;298(6):102024.
40. Kuang S, Zhu B, Zhang J, et al. A photolabile curcumin-diazirine analogue enables phototherapy with physically and molecularly produced light for Alzheimer's disease treatment. *Angew Chem Int Ed Engl*. 2023;62(45):e202312519.
41. Villagra A, Cheng F, Wang HW, et al. The histone deacetylase HDAC11 regulates the expression of interleukin 10 and immune tolerance. *Nat Immunol*. 2009;10(1):92-100.
42. Yang J, Yin W, Van R, et al. Turn-on chemiluminescence probes and dual-amplification of signal for detection of amyloid beta species in vivo. *Nat Commun*. 2020;11(1):4052.
43. Zhang J, Wickizer C, Ding W, et al. In vivo three-dimensional brain imaging with chemiluminescence probes in Alzheimer's disease models. *Proc Nat Acad Sci USA*. 2023;120(50):e2310131120.
44. Mirzaei N, Tang SP, Ashworth S, et al. In vivo imaging of microglial activation by positron emission tomography with [(11)C]PBR28 in the 5XFAD model of Alzheimer's disease. *Glia*. 2016;64(6):993-1006.
45. Kreisl WC, Lyoo CH, Liow JS, et al. (11)C-PBR28 binding to translocator protein increases with progression of Alzheimer's disease. *Neurobiol Aging*. 2016;44:53-61.

SUPPORTING INFORMATION

Additional supporting information can be found online in the Supporting Information section at the end of this article.

How to cite this article: Bai P, Mondal P, Liu Y, et al. HDAC11 displays neuropathological alterations and offers as a novel drug target for Alzheimer's disease. *Alzheimer's Dement*. 2025;21:e14616. https://doi.org/10.1002/alz.14616